Comparison of 3-dimensional and 1-dimensional schemes in the calculation of atmospheric neutrinos

M. Honda and T. Kajita
Institute for Cosmic Ray Research, University of Tokyo, Kashiwa 277-8582, Japan

K. Kasahara
Department of Electronic Information Systems, Shibaura Institute of Technology, Fukasaku, Ohmiya 330-8570, Japan

S. Midorikawa
Faculty of Engineering, Aomori University, Aomori 030-0943, Japan

(Received 30 March 2001; published 10 August 2001)

A 3-dimensional calculation of atmospheric neutrino flux is presented, and the results are compared with those of a 1-dimensional calculation. In this study, the interaction and propagation of particles is treated in a 3-dimensional way including the curvature of charged particles due to the geomagnetic field, which is assumed to be a dipole field. The purpose of this paper is limited to the comparison of calculation schemes. The updated flux value with a new interaction model and primary flux model will be reported in a separate paper. Except for nearly horizontal directions, the flux is very similar to the result of 1-dimensional calculations. However, for near-horizontal directions an enhancement of the neutrino flux is seen even at energies as high as 1 GeV. The production height of neutrinos is lower than the prediction of the 1-dimensional calculation for near-horizontal directions, and is a little higher for near-vertical directions. However, the difference is not evident except for near-horizontal directions.

DOI: 10.1103/PhysRevD.64.053011 PACS number(s): 95.85.Ry, 14.60.Pq, 96.40.Tv

I. INTRODUCTION

The conflict between the experimental data and theoretical predictions of atmospheric neutrinos gives evidence for neutrino oscillations [1] (see also [2–5]). The data from Super-Kamiokande, which dominate the statistics in the atmospheric neutrino data, are well explained by $\nu_\tau \leftrightarrow \nu_\mu$ oscillation with $\Delta m^2 \simeq 3\times 10^{-3}$ eV^2 and $\sin^2 2\theta \sim 1$. We note that the oscillation mode of $\nu_\tau \leftrightarrow \nu_\mu$ with $\Delta m^2 \sim 1 \times 10^{-2}$ eV^2 was suggested [6–8] immediately after the discovery of the atmospheric neutrino anomaly [9], using the atmospheric neutrino flux predicted in the 1-dimensional approximation [10]. The theoretical study of atmospheric neutrinos has also been improved since that time, but most of them still employ the 1-dimensional approximation [11,12]. For further study of neutrino oscillations, a better prediction of the atmospheric neutrino flux calculated using a 3-dimensional scheme may be needed.

The ''3D effects'' are not very large; the bending of muons in the geomagnetic field is ~ 0.1 rad ($\sim 5°$) in the average muon lifetime, and the transverse momentum of a secondary particle in a hadronic interaction is typically 0.3 GeV/c. Both are small effects for neutrinos with an energy of $\gtrsim 1$ GeV, and could be ignored for $\gg 1$ GeV. Therefore it is considered that a 1-dimensional calculation is sufficient for the confirmation of neutrino oscillation and their nonzero masses. The effects become important, however, for neutrinos with energies $\lesssim 1$ GeV.

One of the difficult problems of the 3-dimensional calculation is the computation time. If we sample the cosmic ray uniformly over the surface of the Earth, roughly speaking, only (detector size/Earth radius)^2 of the produced neutrinos go through the detector. The 3-dimensional calculations that have been reported so far adopt some ideas that address this computation problem. Tserkovnyak *et al.* assumed a huge detector size [13]. However, they still suffered from small statistics. On the other hand, Battistoni *et al.* assumed a spherical symmetry ignoring the geomagnetic field in the air [14], and they found an enhancement of atmospheric neutrino fluxes in near-horizontal directions at low energies. This is a general feature in the 3-dimensional calculation; Lipari gives an explanation of it in terms of geometry [15]. This feature is not seen in the 1-dimensional calculation.

In this study, we introduce a dipole geomagnetic field for both the geomagnetic cutoff test and the particle simulation in air. With the axisymmetry of the dipole geomagnetic field, we can integrate the results over longitudinal directions and reduce the computation time to get sufficient statistics. This dipole magnetic field may be an oversimplification for the geomagnetism, but is useful to estimate the effect of the geomagnetic field in the air on atmospheric neutrinos. This is stressed by Lipari [16].

In this paper, we concentrate on a comparison of the 3-dimensional calculation, with and without the geomagnetic field in the air, and the 1-dimensional one. The flux value will be reported in a separate paper with an improved interaction model.

II. SIMULATION SETUP AND PROCEDURE

The atmospheric neutrino flux of $\lesssim 1$ GeV, in which we expect sizable differences between 1-dimensional and 3-dimensional calculations, is mainly produced by the cosmic rays with energies below 100 GeV. The recently observed proton cosmic ray flux in this energy region is lower

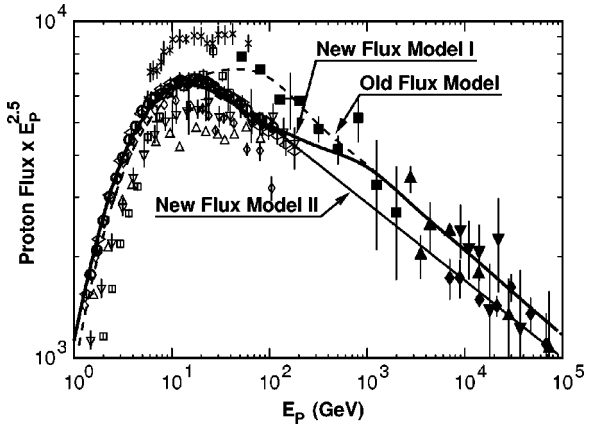

FIG. 1. Primary cosmic ray observation and our model curves for protons at solar minimum. New flux model I is used in this study. Crosses indicate data from Ref. [17], open squares MASS [18], open upward triangles LEAP [19], open downward triangles IMAX [20], open vertical diamonds CAPRICE [21], open circles BESS [22], and open horizontal diamonds AMS [23]. Pluses indicate data from Ref. [24], closed squares Ref. [25], closed vertical diamonds JACEE [26], closed upward triangles Ref. [27], and closed downward triangles Ref. [28].

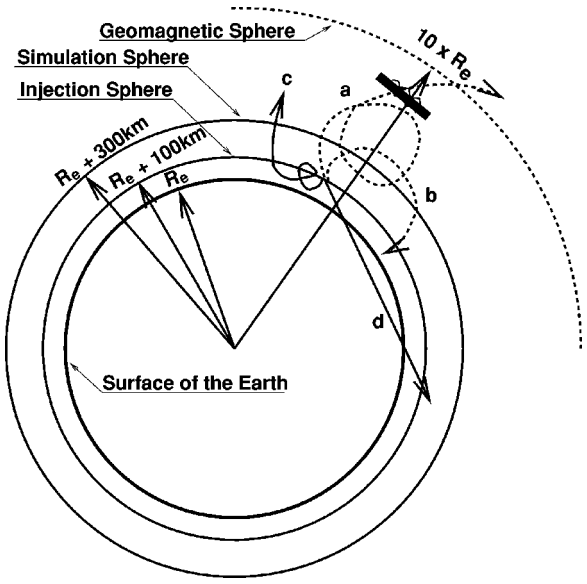

FIG. 2. Schematic view of the 3-dimensional calculation of atmospheric neutrinos. The curves in the figure show (a) the backtracking orbit for an allowed path, (b) same as (a) but for a forbidden path, (c) the orbit of a discarded particle, and (d) the track for neutrinos.

than the Hidaka-Kajita-Kasahara-Midorikawa (HKKM) [11] flux model above 30 GeV, showing a maximum difference of 30% at around 100 GeV (Fig. 1). Variations of the observed flux for <10 GeV are also seen. However, this is mainly due to modulation by solar activity, and the values agree with each other when a proper correction is applied. Therefore, we renew the primary proton flux model based on recent observations, especially those of BESS [22] and AMS [23]. Above 100 GeV, we construct two primary flux models for proton cosmic rays: the new flux model I and new flux model II, shown in Fig. 1 with available data. They are considered as the upper and lower bounds of plausible extrapolation from lower energies. The fraction of heavier chemical composition in cosmic rays is small at <100 GeV, and we take the values of the old HKKM flux model for them.

As a temporary choice, we use the new flux model I in this study. The differences in the primary flux model, including that for heavier nuclei, do not result in large differences in the comparison of 1D and 3D calculation schemes. However, the differences in neutrino flux between the new flux models I, II and the old flux model are briefly addressed in a later section.

For the interaction model, we use the same interaction model as the HKKM calculation [11] in this study. We stress, however, that we are improving the interaction model, since the combination of the new flux model and the present interaction model does not explain the observed flux of secondary cosmic rays at several altitudes. The updated interaction model as well as the primary flux model will be reported in a forthcoming paper with the resulting neutrino flux.

We assume that the surface of the Earth is a simple sphere with radius of $R_e \simeq 6378$ km, and use a geomagnetic coordinate system such that the center of the Earth is the origin and the line from the center of the Earth to the magnetic north pole is the z axis. The geomagnetic field is approximated by a dipole magnetic field as

$$B_x = B_0 3zxR_e^3/r^5, \quad B_y = B_0 3zyR_e^3/r^5, \quad \text{and}$$

$$B_z = B_0(3z^2 - r^2)R_e^3/r^5 \tag{2.1}$$

with $B_0 = -0.30$ G in this coordinate system. The position of the magnetic north pole is calculated to be at (71.4°W, 79.3°N) for the geomagnetic field in 1995, and the magnetic latitudes for SK, Soudan-II, and SNO are 26.9°N, 58°N, and 54.0°N, respectively. The position of SK may be considered as the mid magnetic latitudes (MML), and that of Soudan-II and SNO as the high magnetic latitudes (HML).

In addition to the surface of the Earth, we consider three more spheres. The first one is called the injection sphere with radius of $R_e + 100$ km, the second one is the simulation boundary sphere with radius of $R_e + 300$ km, and the third one is the geomagnetic sphere with radius of $10 \times R_e$. (See Fig. 2.) The simulation of cosmic rays starts at the injection sphere, and is carried out in the space between the surface of the Earth and the simulation boundary sphere. Outside the geomagnetic sphere, we consider the cosmic rays to be free from the effects of the geomagnetic field.

First, the chemical composition and energy are sampled for a cosmic ray following the energy spectrum of each chemical composition. Then the injection position is sampled uniformly over the injection sphere and the arrival directions are sampled so that the zenith angle distribution is proportional to $[\cos\theta(d\cos\theta)]$, where θ is the zenith angle at the injection point. We record the sampled energy, the chemical composition, the position of the injection, and the direction of the cosmic ray, irrespective of the result of the geomagnetic cutoff test.

For the geomagnetic cutoff test, we trace the backward path of a particle with the same mass and energy as the cosmic ray but with the opposite charge. If the particle goes out of the geomagnetic sphere within 100 sec without going into the injection sphere, we judge the cosmic ray has passed the geomagnetic cutoff. The above geomagnetic cutoff test only picks up cosmic rays that arrive in the injection plane for the first time. Note that the geomagnetic cutoff test works exactly the same way for two particles with the same rigidity (p/Z).

The cosmic rays that pass the geomagnetic cutoff test are fed into the COSMOS simulation code [29]. When a neutrino is produced in the simulation, the production position and the direction are recorded. Other particles are traced until they decay, leave the simulation sphere, or enter the Earth.

For the neutrinos, we calculate both the point of entrance into the Earth and the point of emergence from the Earth; neutrinos that do not enter the Earth are discarded. At each point, the arrival zenith angle and he azimuth angles are calculated. We note that the arrival zenith angle is defined as the angle between the downward normal vector direction and the direction of the neutrino at each point. The azimuth angle is defined as the projection angle on the tangential plane at each point.

We refer to the calculation setup explained above as the 3D calculation. We performed three other calculations with different setups from the above. The first is a 1-dimensional calculation such that the geomagnetic cutoff test is applied with the same dipole magnetic field as in the 3-dimensional case, but all particles are treated by COSMOS in a 1-dimensional fashion (1D calculation), in which all secondary particles are produced in the direction of the primary cosmic ray. The second is such that the geomagnetic cutoff and the interaction are treated in the same way as in the 3D calculation but the effect of the geomagnetic field is ignored in the air (3D-nomag calculation). The third is another 1D calculation such that most of the procedures are the same as for the 1D, but the geomagnetic cutoff is applied with the multipole expanded (8th order) geomagnetic field (1D-multipole calculation). This is almost the same as the HKKM calculation [11] except for the flux model. The new flux model I is used for all the above calculations. These calculations are perfomed both for the SK site and for North America.

III. SIMULATION RESULTS

A. Direction averaged flux

In Fig. 3, we show the energy spectra averaged over all directions of atmospheric neutrinos predicted by several different calculations for the MML and in Fig. 4 for HML. To see the difference more clearly, we also calculated the ratios of the 1D, 3D, and 3D-nomag to the 1D-multipole fluxes for MML and HML, and the ratio of 3D fluxes for HML to that for MML in Fig. 5.

The differences between 1D, 3D, 3D-nomag, and 1D-multipole calculations using the same primary cosmic ray flux model are small for the MML. The differences are less than 5% for $\gtrsim 0.2$ GeV for all the calculation schemes, and for $\gtrsim 0.1$ GeV between 1D and 3D. On the other hand, the differences between different calculation schemes are larger in the HML than those in the MML.

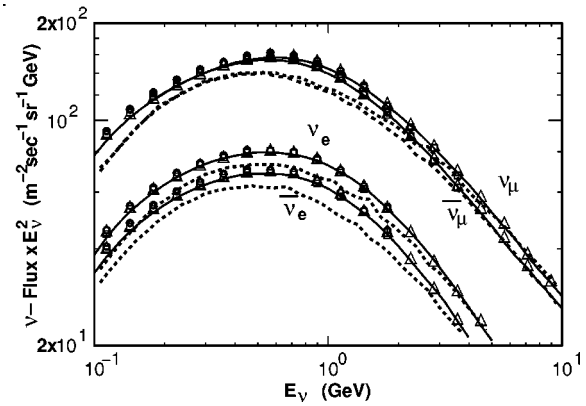

FIG. 3. Direction averaged atmospheric neutrino flux multiplied by E_ν^2 for the MML. The squares are for 3D, triangles for 1D, and circles for 3D-nomag calculations. The solid and dashed lines show the neutrino fluxes of 1D-multipole calculation and Battistoni *et al.* [14], respectively.

The neutrino flux difference between the new flux models I and II is $\lesssim 2-3$ % at 1 GeV and it grows to $\sim 10\%$ at 10 GeV. It is rather small in the energy region where the ''3D effects'' are important. However, the difference between the old flux model and the new flux model I is 8–12 % at 1 GeV and grows to a maximum of $\sim 20\%$ at 6–8 GeV, and then decreases above these energies.

The flux of Battistoni *et al.* [14] is a little smaller than ours for $\lesssim 3$ GeV, and the difference is $\sim 15\%$ at 1 GeV in the MML. In the HML, their flux is again smaller than ours for 0.3 GeV $\lesssim E_\nu \lesssim 3$ GeV ($\sim 15\%$ at 1 GeV), but below 0.3 GeV their flux is similar to or even larger than ours. However, their flux is very similar to ours at energies $\gtrsim 3$ GeV in both the MML and HML.

B. Zenith angle dependence

In the 1-dimensional approximation, and without the geomagnetic cutoff, we expect a larger atmospheric neutrino flux

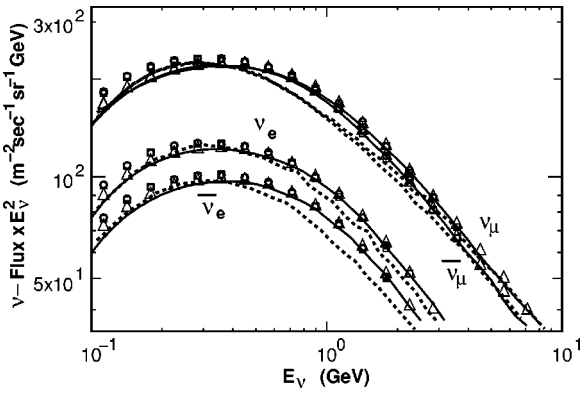

FIG. 4. Direction averaged atmospheric neutrino flux multiplied by E_ν^2 for the HML. The squares are for 3D, triangles for 1D, and circles for 3D-nomag calculations. The solid and dashed lines show the neutrino fluxes of 1D-multipole calculation and Battistoni *et al.* [14], respectively.

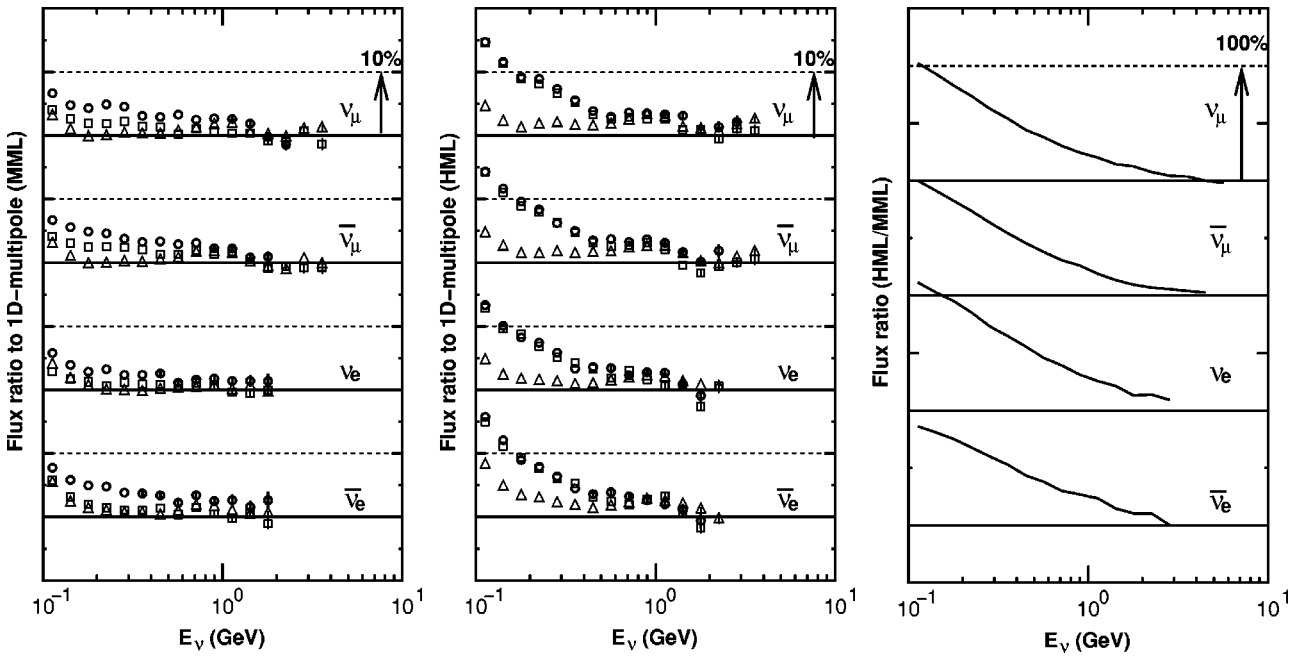

FIG. 5. Flux ratios of 1D, 3D, and 3D-nomag to the 1D-multipole calculation in MML (left) and HML (center), and the ratio of 3D for HML to 3D for MML (right). The squares are for 3D, triangles for 1D, and circles for 3D-nomag calculations.

for the horizontal direction than for the vertical direction. Since the average first interaction point of cosmic rays is ~ 100 g/cm^2 in column density, the inclined cosmic rays produce pions in a higher altitude than the vertical ones. When π-μ decays take place in the dense air, the resulting neutrino flux is reduced, since the interaction probability of pions with the other air nuclei and the energy loss of the muons increase with increasing air density. Note, however, that the muon energy loss is more important than the interaction probability of pions in the energy region in which we are interested ($\lesssim 1$ GeV).

The geomagnetic cutoff modifies the zenith angle dependence of the atmospheric neutrino flux at low energies ($\lesssim 3$ GeV). In the MML, even high rigidity particles ($\gtrsim 35$ GV) do not pass the geomagnetic cutoff test in the near-horizontal easterly directions, while relatively low rigidity particles (~ 11 GV) pass the test in the near-vertical directions. Thus the atmospheric neutrino flux for horizontal directions is lower than that for the neighboring directions, even after averaging over all azimuth angles. In the HML, we expect the downward going neutrino flux to be larger than the upward going neutrino flux, since the averaged cutoff rigidity is lower for down going directions.

We show the zenith angle variation calculated in the 1D, 3D, and 3D-nomag schemes in Figs. 6 and 7 for the MML and HML, respectively, to compare the zenith angle dependence of the atmospheric neutrino flux among different calculation schemes. The neutrino fluxes are integrated in the energy ranges of 0.1–0.3 GeV, 0.3–1 GeV, and 1–3.1 GeV, and averaged over all azimuth angles.

The zenith angle variations of the atmospheric neutrino fluxes calculated in the 1D and 1D-multipole schemes are well explained by the incident angle of the primary cosmic ray and the geomagnetic cutoff as above. In the 3D and 3D-nomag calculations, however, there is a large enhancement of neutrino fluxes in the near-horizontal directions, which is not seen in the 1D and 1D-multipole calculations. This horizontal enhancement is seen in both the MML and HML. The horizontal enhancement of atmospheric neutrino flux was first reported by Battistoni *et al.* [14], and Lipari gave an explanation in terms of geometry [15].

For comparison with the results of Battistoni *et al.* [14], we plotted their results alongside our 3D-nomag results, since they considered the geomagnetic field outside the atmosphere to calculate the geomagnetic cutoff but they did not apply the geomagnetic field in the atmosphere. We found that the horizontal enhancement is $\sim 10\%$ larger than ours. However, this is not considered to be the result of the difference between the multipole and dipole geomagentic cutoff schemes. The 1D calculation gives a larger flux than the 1D-multipole calculation at near-horizontal directions in our study. Therefore, we conclude that the larger horizontal enhancement in the results of Battistoni *et al.* can be explained by the difference of their hadronic interaction model from ours, especially as regards the transverse momentum of secondary pions.

C. East-west effect

We show the azimuth variation of the neutrino fluxes calculated in 1D, 3D, and 3D-nomag schemes in Fig. 8 and Fig. 9 for the MML and HML, respectively. The azimuth variation calculated in the 1D-multipole scheme is also shown with that in the 1D scheme as a histogram. The neutrino flux is integrated over the energy ranges of 0.1–0.3 GeV, 0.3–1 GeV, and 1–3.1 GeV, and averaged over the zenith angles $|\cos(\theta_{\rm Zenith})| < 0.5$.

The azimuthal variation of the neutrino fluxes is determined only by the geomagnetic cutoff in the 1-dimensional

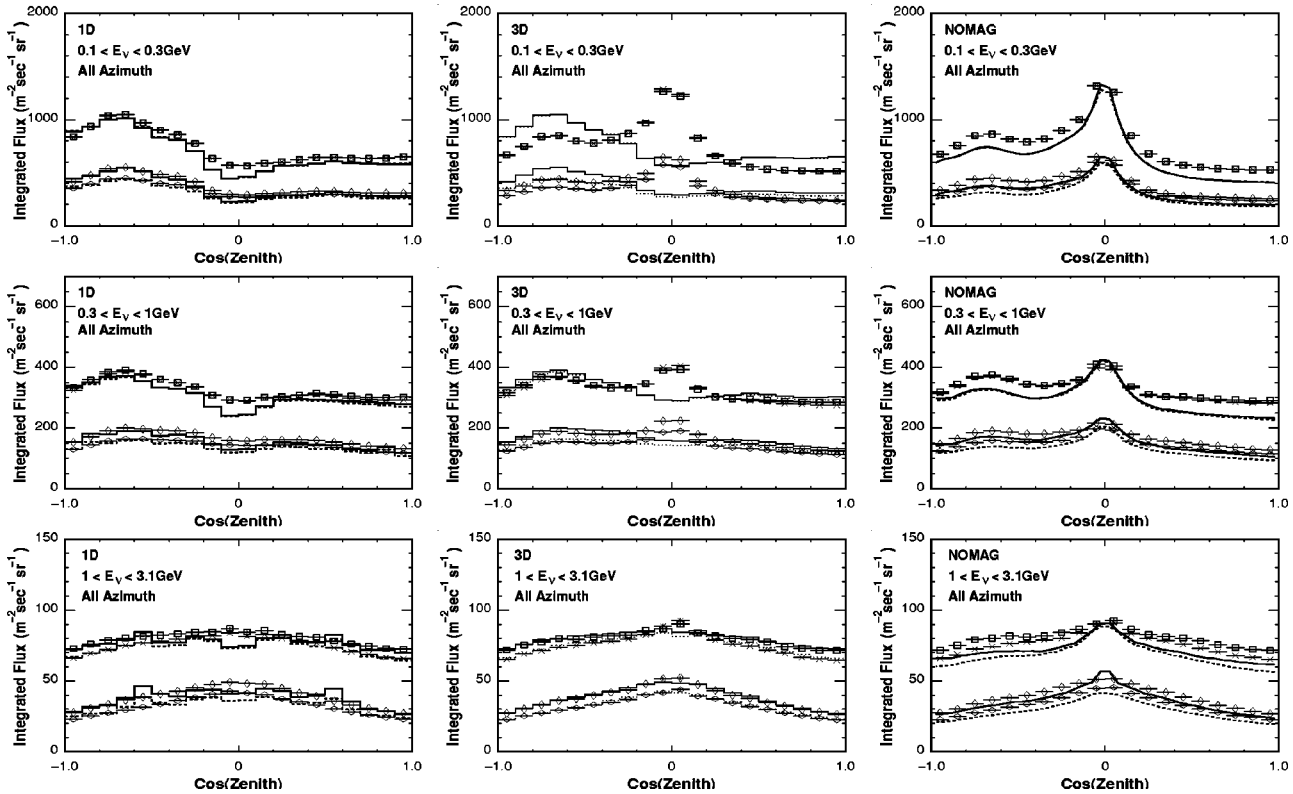

FIG. 6. Zenith angle dependence of atmospheric neutrino flux calculated in the 1D (left), 3D (center), and 3D-nomag (right) schemes for the MML. Squares are for ν_μ, asterisks for $\overline{\nu}_\mu$, vertical diamonds for ν_e, and horizontal diamonds for $\overline{\nu}_e$. The solid line histograms in 1D figures show the ν fluxes, and the dotted ones the $\overline{\nu}$ fluxes for the 1D-multipole calculation. The solid lines in 3D-nomag figures show the ν fluxes, and the dotted lines the $\overline{\nu}$ fluxes from Ref. [14]. The neutrino fluxes are integrated in the energy ranges of 0.1–0.3 GeV, 0.3–1 GeV, and 1–3.1 GeV, and averaged over all the azimuth angles. Cos(zenith)$=1$ is for the downward going neutrinos. The results of the 1D calculation are also plotted in the 3D figure as a solid line histogram for ν and dotted line histogram for $\overline{\nu}$ for comparison.

approximation, and we expect only a small deviation from that in the 3-dimensional schemes. (For detailed discussions, see Lipari *et al.* [30].) The difference between 1D, 3D, and 3D-nomag results is small since they use the same geomagnetic cutoff scheme. The difference between the dipole and multipole geomagnetic cutoff schemes is also small. Note that there is an experimental study of the azimuth variation of the atmospheric neutrino flux [31], although the statistics in this study is small.

In both the MML and HML, the atmospheric neutrino fluxes are larger in the westerly directions ($180°<$azimuth $<360°$) than the easterly directions ($0°<$azimuth$<180°$) due to the lower cutoff rigidity for the westerly directions. However, the difference between the westerly direction and the easterly direction is smaller in the HML than in the MML. Since the corresponding energy to the cutoff rigidity is near to or even lower than the pion production threshold of cosmic rays in the HML, the effect of the geomagnetic cutoff is small.

We would like to note, however, that there is a feature which is not explained by the geomagnetic cutoff only. The azimuth variation of $\overline{\nu}_\mu$ and ν_e fluxes is larger than that of ν_μ and $\overline{\nu}_e$ fluxes only in the 3D calculation, and this is not seen in other calculation schemes. The differences betweeen ν_μ and $\overline{\nu}_\mu$ and ν_e and $\overline{\nu}_e$ are considered to result from the curvature of muons in the geomagnetic field. This feature is seen in both the HML and MML.

In order to study the horizontal enhancement in more detail, we have taken the flux ratio between the 3D and 3D-nomag calculations and the 1D calculation for the MML. The flux ratio is shown separately in Fig. 10 for easterly directions (S-E-N 180° in azimuth angle), and in Fig. 11 for westerly directions (N-W-S 180° in azimuth angle). Note that the units of the vertical axis are different in these ratio figures.

First, the amplitude of the horizontal enhancement is different in easterly and westerly directions for both 3D and 3D-nomag calculations. In the near-horizontal easterly directions, it is $\sim$200% for 0.1–0.3 GeV and $\sim$50% for 0.3–1.0 GeV, while in the westerly directions, it is $\sim$100% for 0.1–0.3 GeV, and $\sim$30% for 0.3–1 GeV. The large amplitude of the horizontal enhancement in the easterly direction is caused by the low neutrino flux in the 1D calculation in near-horizontal easterly directions due to the high cutoff rigidity ($\gtrsim$35 GV). The ''3D effects'' work to smear out such a quick variation, and the ratio of the 3D to the 1D flux is larger for the region with higher cutoff rigidity if the zenith angle is the same.

In the energy range of 1.0–3.1 GeV, however, the horizontal enhancement becomes small and the difference between 3D and 3D-nomag calculations becomes apparent. In

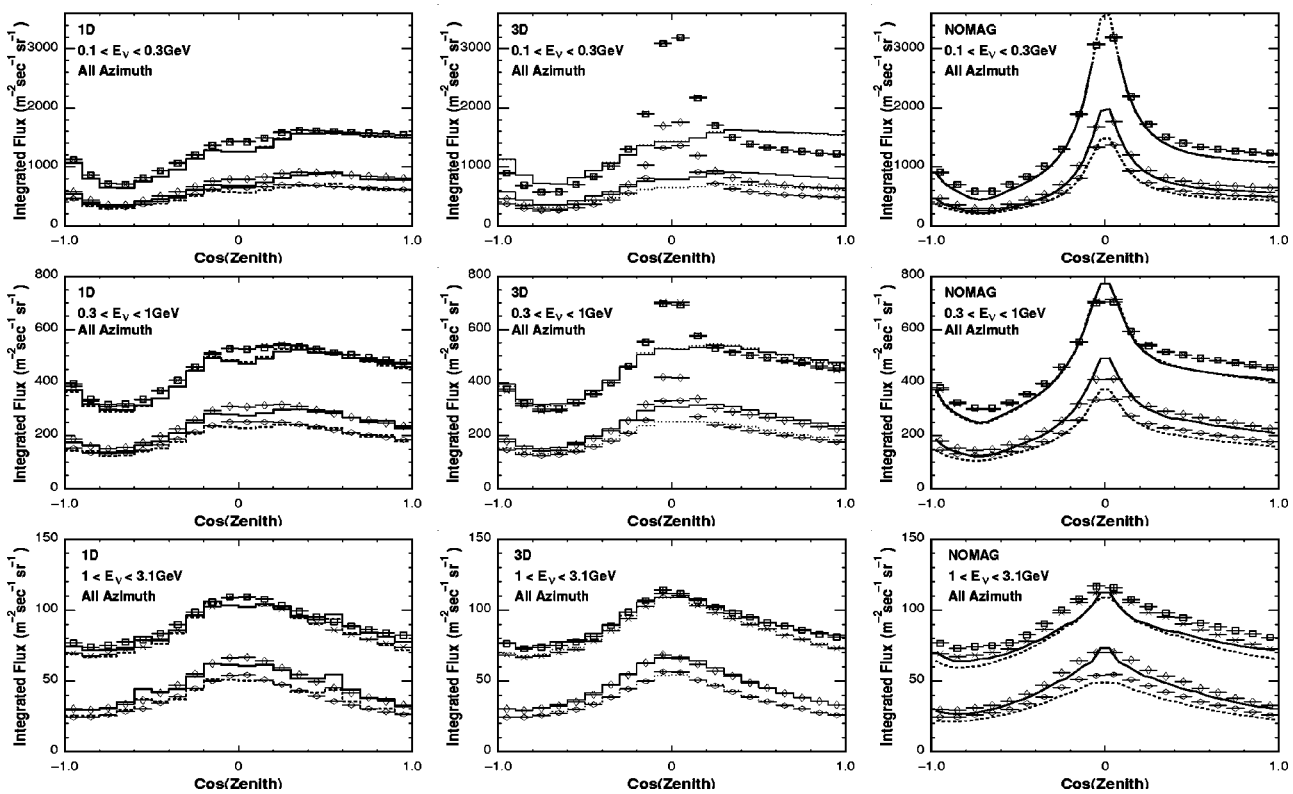

FIG. 7. Zenith angle dependence of atmospheric neutrino flux calculated in the 1D (left), 3D (center), and 3D-nomag (right) schemes for the HML. Squares are for ν_μ, asterisks for $\overline{\nu}_\mu$, vertical diamonds for ν_e, and horizontal diamonds for $\overline{\nu}_e$ for 1D, 3D, and 3D-nomag calculations. The solid line histograms in 1D figures show the ν fluxes, and the dotted ones the $\overline{\nu}$ fluxes for the 1D-multipole calculation. The solid lines in 3D-nomag figures show the ν fluxes, and the dotted lines the $\overline{\nu}$ fluxes from Ref. [14]. The neutrino fluxes are integrated in the energy ranges of 0.1–0.3 GeV, 0.3–1 GeV, and 1–3.1 GeV, and averaged over all the azimuth angles. Cos(zenith) = 1 is for the downward going neutrinos. The results of the 1D calculation are also plotted in the 3D figure as the solid line histogram for ν and dotted line histogram for $\overline{\nu}$ for comparison.

the 3D calculation, ν_μ and $\overline{\nu}_e$ fluxes are enhanced while $\overline{\nu}_\mu$ and ν_e fluxes are suppressed for the easterly horizontal direction, and $\overline{\nu}_\mu$ and ν_e fluxes are enhanced while ν_μ and $\overline{\nu}_e$ fluxes are suppressed for the westerly horizontal direction. This feature is not seen in the 3D-nomag calculation. Remember the fact that both the $\overline{\nu}_\mu$ and ν_e are produced in a μ^+ decay, while both the ν_μ and $\overline{\nu}_e$ are produced in a μ^- decay. This enhancement and suppression are related to the muon curvature in the geomagnetic field.

A muon is produced in a direction following the P_t distribution of pions in the hadronic interaction of the parent cosmic ray. The directions of the potential parent cosmic rays of a muon have an axisymmetric distribution around the muon direction at the muon production point, ignoring the bending of pions in the geomagnetic field. For near-horizontal muons, therefore, some of the potential parent cosmic rays are shaded by the Earth. Since a muon changes its direction by $\sim 5°$ within its average lifetime in the geomagnetic field, the shading of the cosmic ray by the Earth works in different way depending on the direction and charge of the muons. For easterly μ^+ and westerly μ^-, the shading by the Earth works more effectively, and the neutrinos produced by these muons are suppressed. For easterly μ^- and westerly μ^+, the shading by the Earth works less effectively, and the neutrinos produced by these muons are enhanced. Note that the shading by the Earth reduces the neutrino flux near the horizontal directions, but is not seen in the resulting neutrino flux due to the large horizontal enhancement.

There is an additional effect related to the geomagnetic cutoff. The geomagnetic cutoff applied to the parent cosmic ray is different between 3D and 3D-nomag calculations due to the muon curvature. Generally speaking, a higher cutoff rigidity is applied to a μ^+ and a lower rigidity cutoff is applied to a μ^-, irrespective of direction. However, this effect is not evident except for the easterly and near-horizontal directions, where the cutoff rigidity rapidly increases toward the horizontal direction.

The amplitudes of the enhancement or suppression in the geomagnetic field are $\sim 5\%$ for the ν_μ and $\sim 10\%$ for the $\overline{\nu}_\mu$, 20–30 % for ν_e and 10–20 % for $\overline{\nu}_e$, over a wide energy range in the near-horizontal westerly or easterly direction. These amplitudes can be understood by the muon curvature effect explained above. Note that Lipari pointed out the importance of the magnetic field after the geomagnetic cutoff in Ref. [16].

For the HML, the flux ratio is also calculated and shown separately in Fig. 12 for easterly directions (S-E-N 180° in

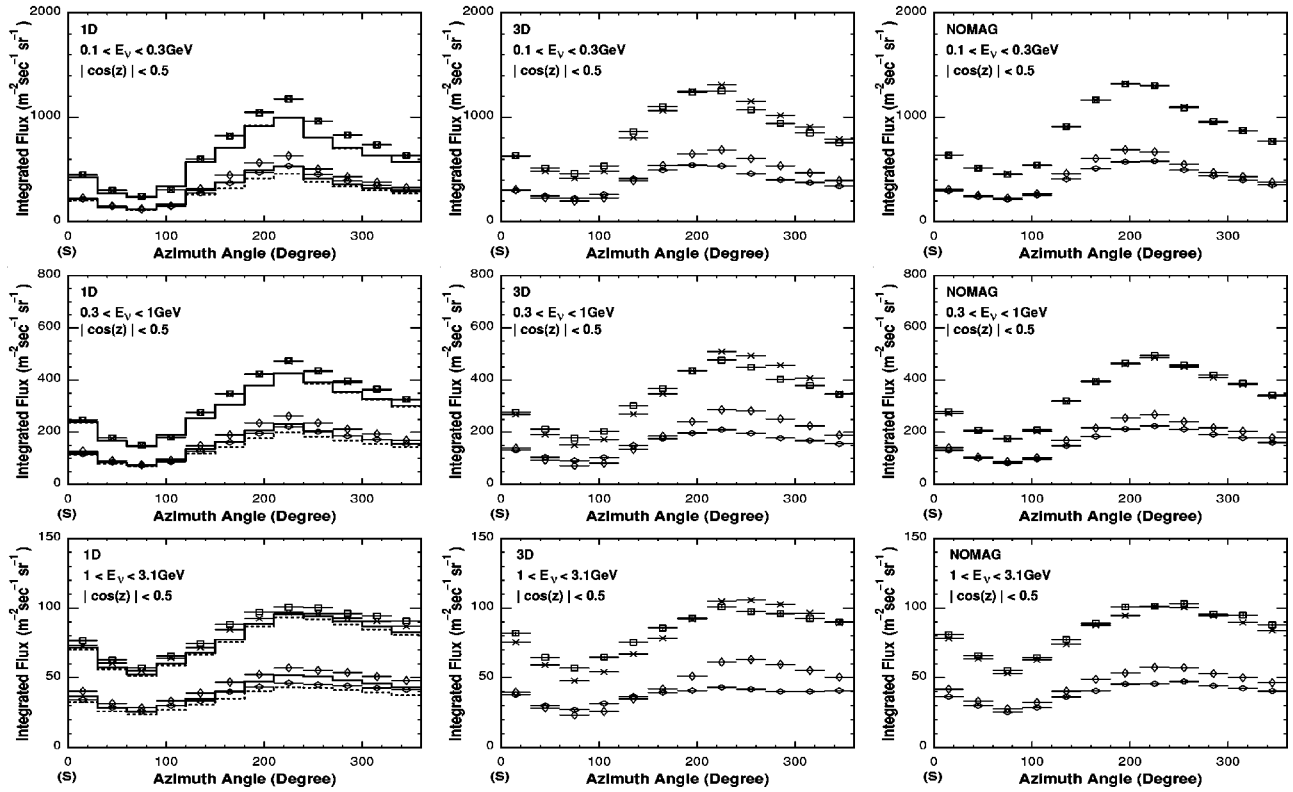

FIG. 8. Azimuth dependence of atmospheric neutrino fluxes calculated in the 1D (left), 3D (center), and 3D-nomag (right) schemes for the MML. Squares are for ν_μ, asterisks for $\overline{\nu}_\mu$, vertical diamonds for ν_e, and horizontal diamonds for $\overline{\nu}_e$. The neutrino fluxes are integrated over the energy ranges of 0.1–0.3 GeV, 0.3–1 GeV, and 1–3.1 GeV, and averaged over the zenith angles $|\cos(\theta_{\rm Zenith})|<0.5$. The results of the 1D-multipole calculation are plotted in the 1D figures; the solid lines show the ν fluxes, and the dotted line the $\overline{\nu}$ fluxes. Azimuth $=0$, 90, 180, 270 are the magnetic southerly, easterly, northerly, and westerly directions, respectively.

azimuth angle), and Fig. 13 for westerly directions (N-W-S 180° in azimuth angle). Note that the units of the vertical axis are different in these ratio figures.

The general features are the same as in the MML, but the horizontal enhancement is larger for lower neutrino energies, and the difference between 3D and 3D-nomag calculations is seen in the near-horizontal directions for $\gtrsim 1$ GeV. However, the difference between easterly and westerly directions is smaller than that in the MML, since the effect of the rigidity cutoff is small even in the near-horizontal directions. It is $\sim$100% for 0.1–0.3 GeV, and $\sim$30% for 0.3–1 GeV for both directions. The differences of the fluxes in 3D and 3D-nomag calculation are also similar to those in the MML, but a little smaller.

D. Neutrino production height

As we have already discussed in Sec. III B, the production height of atmospheric neutrinos is mainly determined by the zenith angle of incoming cosmic rays in the 1D calculation. The cutoff rigidity also gives an additional effect to the production height for low energy neutrinos. The production height of a fixed energy neutrino is lower for higher energy parent cosmic rays, since the interaction-decay cascade extends deeper into the atmosphere when it is initiated by higher energy cosmic rays. The production height is also different for different kinds of neutrino. It is lower for ν_e and $\overline{\nu}_e$ than for ν_μ and $\overline{\nu}_\mu$, because the former are mainly produced only in the decay of muons and the latter are produced in both the muon and pion decays, and the muons are mainly produced in the pion decay.

In order to study the difference in the production height between the 1D and 3D calculations, we integrate it from ground level to the top of the atmosphere for the 1D and 3D calculations. We show the accumulated probabilities of 20%, 50% (median), and 80% in Figs. 14 and 15.

We find that the production heights in the 3D and 1D calculations are almost identical for the near-vertical directions. They also roughly agree with each other for the near-horizontal directions at high energies ($\gtrsim 1$ GeV). However, the production height in the 3D calculation is apparently lower than that in the 1D calculation for near-horizontal directions and neutrino energies <1 GeV. Despite this difference, the essential discussions for the production height in the 1D calculation can be applied to the 3D calculation. The production height for the near-vertical direction is lower than that for the near-horizontal direction. The effect of the geomagnetic cutoff on the production height can also be seen in the comparison of the MML and HML, and in the comparison of easterly and westerly near-horizontal directions.

From these figures, we find that the neutrino production heights calculated in the 1D and 3D calculations agree with each other for >0.3 GeV in the near-vertical direction, and

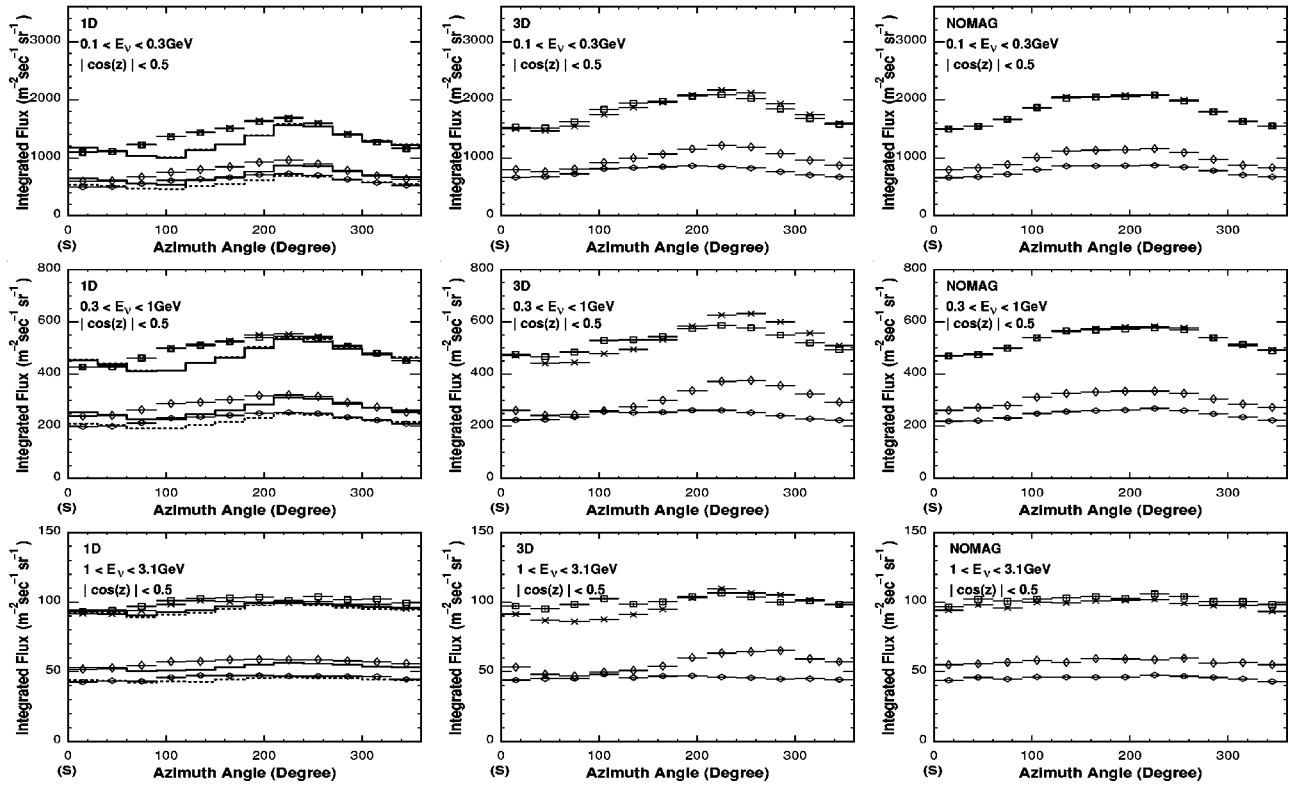

FIG. 9. Azimuth dependence of atmospheric neutrino flux calculated in the 1D (left), 3D (center), and 3D-nomag (right) procedures for the HML. Squares are for ν_μ, asterisks for $\bar{\nu}_\mu$, vertical diamonds for ν_e, and horizontal diamonds for $\bar{\nu}_e$. The neutrino flux is integrated over the energy ranges of 0.1–0.3 GeV, 0.3–1 GeV, and 1–3.1 GeV, and averaged over the zenith angles $|\cos(\theta_{\text{Zenith}})|<0.5$. The results of the 1D-multipole calculation are plotted in the 1D figures; the solid lines show the ν fluxes, and the dotted line the $\bar{\nu}$ fluxes. Azimuth $=0$, 90, 180, 270 are the magnetic southerly, easterly, northerly, and westerly directions, respectively.

for >1 GeV in near-horizontal direction. Note that at high energies ($\gtrsim 2$ GeV) our calculation also suffers from small statistics. However, in the near-horizontal direction and for <1 GeV, the production height is lower in the 3D calculation than that in the 1D calculation. The difference of the production heights between the decay products of μ^- (ν_μ and $\bar{\nu}_e$) and those of μ^+ ($\bar{\nu}_\mu$ and ν_e) is also seen in the 3D calculation at energies of $\gtrsim 0.3$ GeV. The production height of ν_μ or $\bar{\nu}_e$ is higher than that of $\bar{\nu}_\mu$ or ν_e for the westerly direction, and the production height of ν_μ or $\bar{\nu}_e$ is lower than that of $\bar{\nu}_\mu$ or ν_e for the easterly direction. This can be understood by the curvature of muons.

Gaisser and Stanev stressed the importance of the produc-

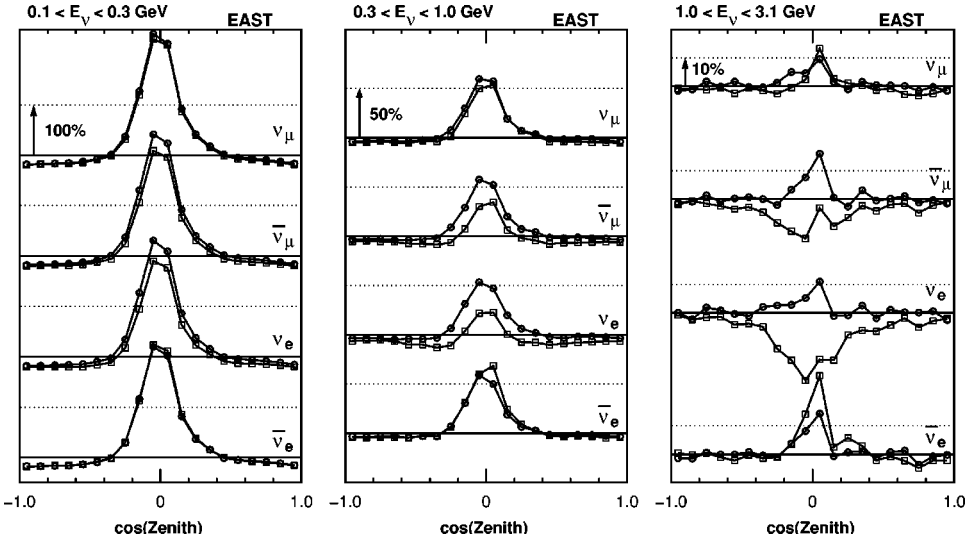

FIG. 10. The ratios of the neutrino fluxes in the 3D and 3D-nomag calculations to that in the 1D calculation for the MML for three energy bands: 0.1–0.3 GeV (left), 0.3–1 GeV (center), and 1–3.1 GeV (right) in the easterly directions. Squares indicate 3D to 1D ratios and circles 3D-nomag to 1D ratios. The scales are different for each energy band.

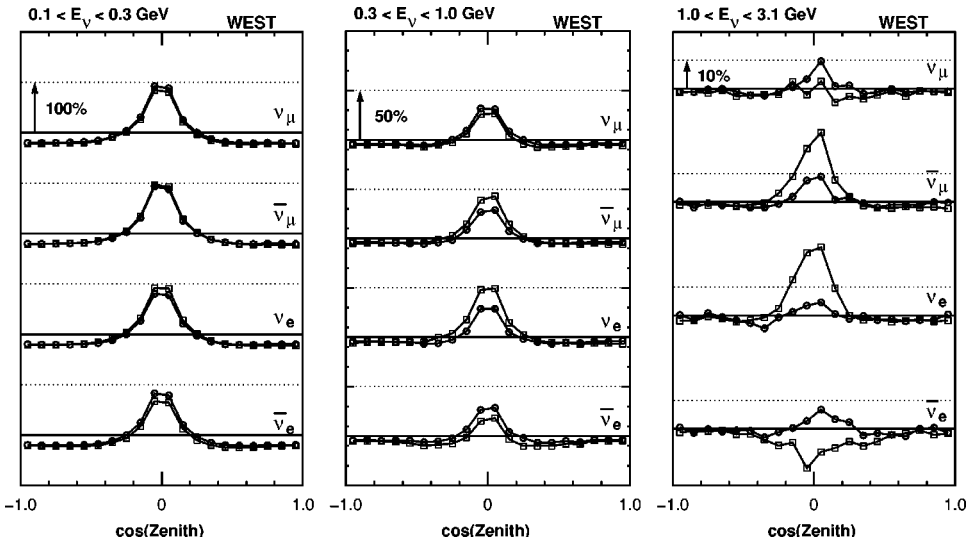

FIG. 11. The ratios of the neutrino fluxes in the 3D and 3D-nomag calculations to that in the 1D calculations for the MML for three energy bands: 0.1–0.3 GeV (left), 0.3–1 GeV (center), and 1–3.1 GeV (right) in the westerly directions. Squares indicate 3D to 1D ratios and circles 3D-nomag to 1D ratios. The scales are different for each energy band.

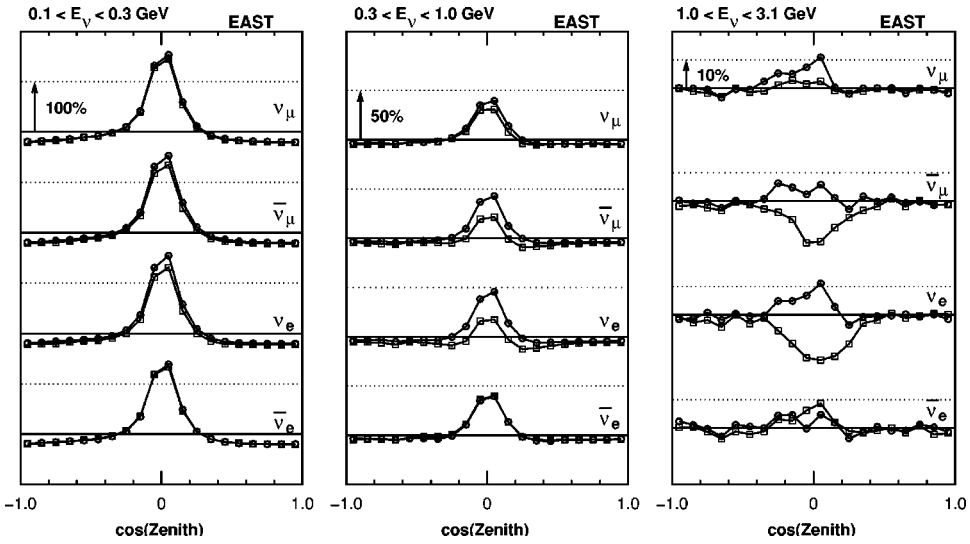

FIG. 12. The ratios of the neutrino fluxes in the 3D and 3D-nomag calculations to that in the 1D calculation for the HML for three energy bands: 0.1–0.3 GeV (left), 0.3–1 GeV (center), and 1–3.1 GeV (right) in the easterly directions. Squares indicate 3D to 1D ratios and circles 3D-nomag to 1D ratios. The scales are different for each energy band.

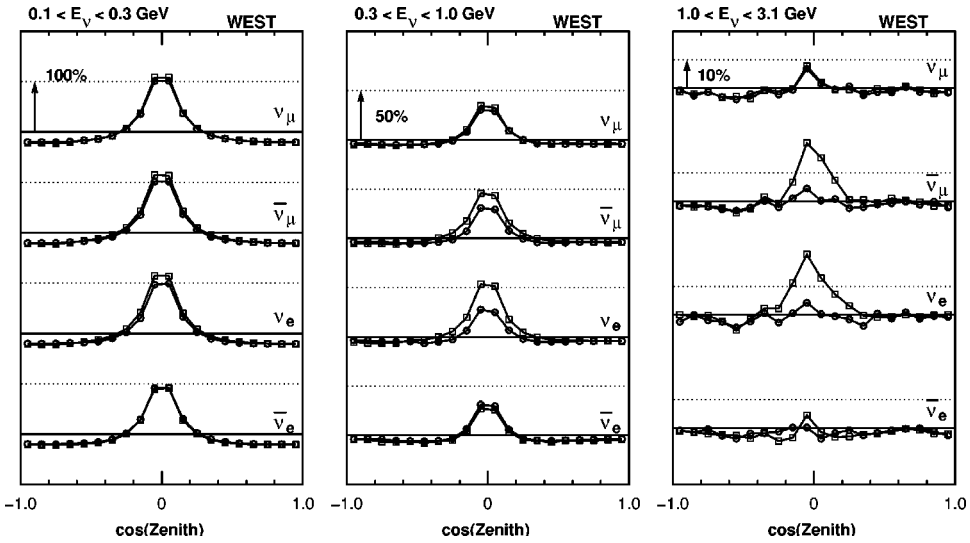

FIG. 13. The ratios of the neutrino fluxes in the 3D and 3D-nomag calculations to that in the 1D calculation for the HML for three energy bands: 0.1–0.3 GeV (left), 0.3–1 GeV (center), and 1–3.1 GeV (right) in the westerly directions. Squares indicate 3D to 1D ratios and circles 3D-nomag to 1D ratios. The scales are different for each energy band.

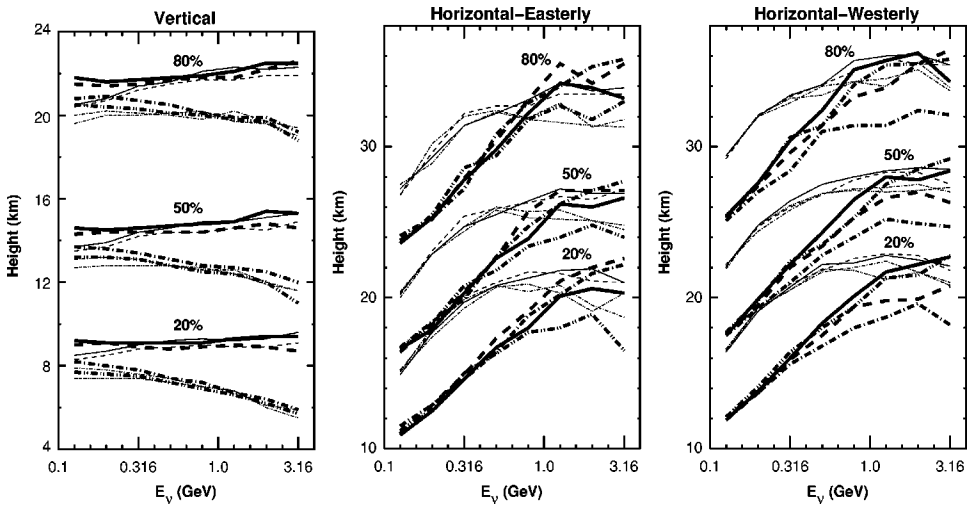

FIG. 14. Constant accumulation probability line for neutrino production height for near-vertical [$|\cos(\text{zenith})|>0.9$] (left), near-horizontal [$|\cos(\text{zenith})|<0.1$] easterly (center), and near-horizontal westerly (right) directions for the MML. Thick solid lines are for ν_μ, thick dashed lines for $\overline{\nu_\mu}$, thick dash-dotted lines for ν_e, and thick dash-double-dotted lines for $\overline{\nu_e}$ by the 3D calculation. Thin solid lines are for ν_μ, thin dashed lines for $\overline{\nu_\mu}$, thin dash-dotted lines for ν_e, and thin dash-double-dotted lines for $\overline{\nu_e}$ by the 1D calculation.

tion height and the path length in the study of neutrino oscillations [32]. We compare the path length calculated in the 1D and 3D calculations, converting the median production height to the path length by a simple relation,

$$d=\sqrt{(h^2+2R_e h)+(R_e\cos\theta)^2}-R_e\cos\theta, \qquad (3.1)$$

where h is the height, R_e is the radius of the Earth, and d is the path length. We show the ratio of the two path lengths (3D/1D) as a function of cos(zenith) in Fig. 16. In this comparison, we integrated over all the azimuth angles.

At near-horizontal directions the production distance of 0.3 GeV neutrinos is $\sim$10% smaller for the 3D calculation than for the 1D at near-horizontal directions. However, the difference is small, $\lesssim$5%, for 1 GeV neutrinos, as is expected from comparison of the production height. There is almost no difference between the MML and HML in this comparison.

IV. SUMMARY AND DISCUSSION

We have calculated the flux of atmospheric neutrinos in a 3-dimensional scheme (3D), with the geomagnetic field simplified by a dipole approximation. We have made two other calculations using the same geomagnetic cutoff scheme: one is a 1-dimensional scheme (1D) and the other a 3-dimensional calculation without the geomagnetic field in the air (3D-nomag). Adding to the above three, we have prepared another 1-dimensional calculation using the geomag-

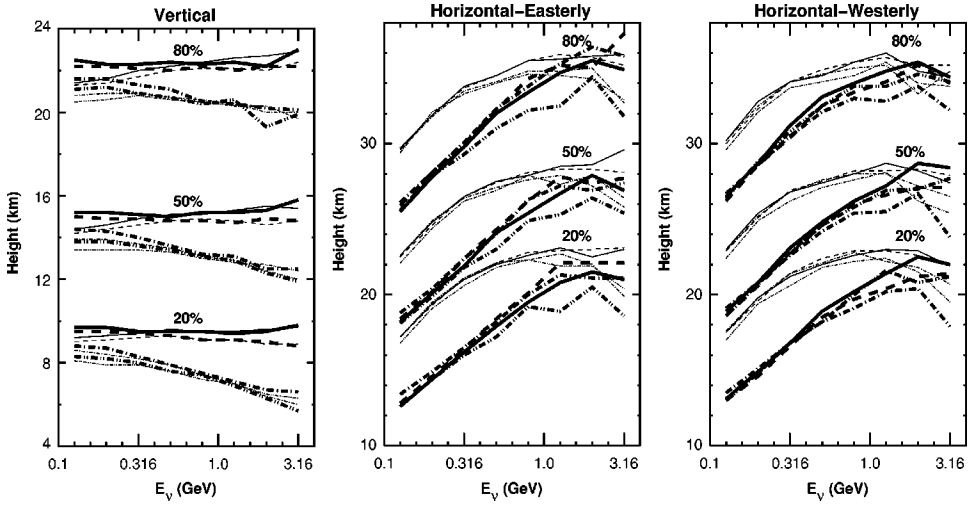

FIG. 15. Constant accumulation probability line for neutrino production height for near-vertical [$|\cos(\text{zenith})|>0.9$] (left), near-horizontal [$|\cos(\text{zenith})|<0.1$] easterly (center), and near-horizontal westerly (right) directions for the HML. Thick solid lines are for ν_μ, thick dashed lines for $\overline{\nu_\mu}$, thick dash-dotted lines for ν_e, and thick dash-double-dotted lines for $\overline{\nu_e}$ by the 3D calculation. Thin solid lines are for ν_μ, thin dashed lines for $\overline{\nu_\mu}$, thin dash-dotted lines for ν_e, and thin dash-double-dotted lines for $\overline{\nu_e}$ by the 1D calculation.

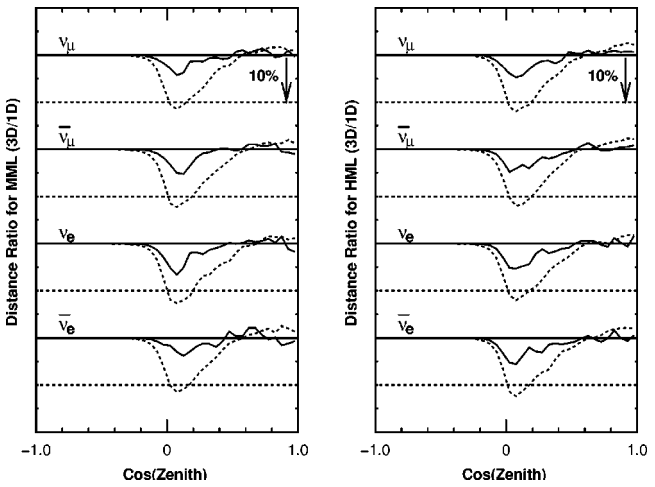

FIG. 16. Ratio of the median path length in 3D calculation to that in 1D calculation for both MML (left) and HML (right). Solid lines show the ratio for 1 GeV neutrinos, and dotted lines for 0.3 GeV neutrinos. $\cos\theta=1$ denotes the downward direction for neutrinos.

netic cutoff scheme due to a multipole expanded geomagnetic field similar to the HKKM calculation [11] (1D-multipole).

The most remarkable fact is the large enhancement of the low energy neutrino flux at near-horizontal directions found in both the 3D and 3D-nomag calculations in both mid and high magnetic latitudes. This enhancement was already reported in other 3-dimensional calculations [14,15], and Lipari showed that the enhancement can be explained by the geometry [15].

We introduce an explanation that is a little different from that by Lipari. We simplify the 1D calculation, assuming that the atmospheric neutrino is produced at a fixed height h, or on a sphere with the radius of R_e+h. We also ignore the geomagnetic cutoff and the zenith angle dependence of production. As primary cosmic rays arrive uniformly on the sphere, the neutrino is also produced uniformly at the sphere for the downward direction. The directional distribution is proportional to

$$(\cos\theta)d(\cos\theta)dS \quad (\cos\theta>0), \tag{4.1}$$

where θ is the zenith angle of the neutrino. Note that we take $\cos\theta>0$ as the downward direction, and we integrate over the azimuth angles.

In the 3D calculation, the neutrino is produced in a little different direction from the primary cosmic ray direction. The directional distribution is calculated by a convolution at the production place, and is proportional to

$$\int_{\cos\theta'>0} D(\theta,\theta')(\cos\theta')d(\cos\theta')d(\cos\theta)dS, \tag{4.2}$$

where θ and θ' are the zenith angles for the neutrino in the case of 3D and 1D calculations, respectively, and $D(\theta,\theta')$ is a dispersion function due to the ''3D effects.'' It is important that Eq. (4.2) gives a nonzero value at $\cos\theta=0$, unless $D(\theta,\theta')$ is a δ-function. The ratio $D(\theta,\theta')\cos\theta'/\cos\theta$ has a divergence at $\cos\theta=0$. The zenith angle θ is almost the same as the arrival direction at the ground; however, $\cos\theta$ can never be 0 for neutrinos which are observed at ground level. The horizontal direction at the ground level actually corresponds to $\cos(\theta)=\sqrt{1-[R_e/(R_e+h)]^2}$ at the production sphere. We do not see a divergence but rather an enhancement of the neutrino flux in the horizontal directions.

For neutrinos with energies >1 GeV, $D(\theta,\theta')$ is well approximated by the δ-function. However, as long as $D(\theta,\theta')$ has a structure extended by more than $\Delta\theta=90°-\cos^{-1}\{\sqrt{1-[R_E/(R_E+h)]^2}\}\sim 5°$, a flux enhancement at horizontal directions would be seen. Thus, although ''3D effects'' are small, they are enhanced by the geometry.

When we compare the 1D and 3D calculations averaged over all directions (Fig. 5), we find that the difference is rather small, and the 3D calculation gives a result $\sim 5\%$ larger than the 1D even at 0.1 GeV for the MML (SK). It is also true that the difference between the calculation with the axisymmetric dipole geomagnetic cutoff (1D) and the multipole geomagnetic cutoff (1D-multipole) is small; 1D gives a $\sim 5\%$ smaller flux than the 1D-multipole calculation. Considering these facts, we can conclude that the 1-dimensional calculation made in [11] is reasonably justified for the MML (SK) as far as the average over all directions is concerned. We note, however, that this is not a general statement; the 3D calculation for the HML (Soudan-II and SNO) gives $\sim 5\%$ higher flux at 0.3 GeV and $\sim 10\%$ higher flux at 0.1 GeV. Thus, the ''3D effects'' work more effectively in the HML than in the MML, or for the position with lower cutoff rigidities.

The effect of the geomagnetic field is different for the neutrinos produced by μ^+ ($\bar{\nu}_\mu$ and ν_e) and the neutrinos produced by μ^- (ν_μ and $\bar{\nu}_e$), as is also predicted by Lipari [16]. This effect is not as large as the geometric enhancement for <1 GeV. However, it gives a 5–30 % effect depending on the kind of neutrinos for near-horizontal directions, and is almost independent of the neutrino energy and magnetic latitude. Since this is caused by the curvature of muons in the geomagnetic field, it will affect neutrino fluxes up to energies of $\gtrsim 10$ GeV.

The comparison of the 3D and 3D-nomag calculations in the overall direction average is also interesting. The variation of the cosmic ray shading by the muon curvature discussed in Sec. III B works in different ways in the easterly and westerly directions. We expect that the difference betwen 3D and 3D-nomag calculations are small due to the compensation of the effects in the two directions. This is true in the calculation in the HML; they agree with each other within the statistical errors. In the MML, however, the neutrino flux is 2–3 % smaller in the 3D calculation than in 3D-nomag at $\lesssim 0.3$ GeV even in the all direction average (Fig. 5). The coupled effect of muon curvature and geomagnetic cutoff may explain this fact, since the cutoff rigidity ($\gtrsim 10$ GV) and the effect work more effectively at the MML.

The production heights of the atmospheric neutrino in the 3D calculation are similar to those in the 1D calculation for

>1 GeV. They are almost identical in the near-vertical directions. In the near-horizontal directions, however, the production height in the 3D calculation is lower than that in the 1D calculation, and there are apparent differences in the production heights between ν_μ and $\overline{\nu_\mu}$ and between ν_e and $\overline{\nu_e}$ due to curvature of muons in the geomagnetic field.

The path length of the atmospheric neutrino is also compared in the 1D and 3D calculations, integrating all azimuth directions. The maximum difference is seen at a near-horizontal direction, and is $\sim 10\%$ for 0.3 GeV neutrinos and $\sim 5\%$ neutrinos. For higher energy neutrinos ($\gg 1$ GeV), we expect very small differences between 1D and 3D calculations.

ACKNOWLEDGMENTS

We are grateful to P. Lipari, A. Okada, and J. Nishimura for useful discussions and comments. We thank S. Orito and T. Sanuki for showing us their data before publication and for discussions. We also thank C. T. Taylor for a careful reading of the manuscript. This work is partly supported by Grants-in-Aid for Scientific Research on Priority Area A (No. 12047227).

[1] Super-Kamiokande Collaboration, Y. Fukuda *et al.*, Phys. Rev. Lett. **81**, 1562 (1998).
[2] Kamiokande Collaboration, K. S. Hirata *et al.*, Phys. Lett. B **280**, 146 (1992); Y. Fukuda *et al.*, *ibid.* **335**, 237 (1994).
[3] IMB Collaboration, D. Casper *et al.*, Phys. Rev. Lett. **66**, 2561 (1991); R. Becker-Szendy *et al.*, Phys. Rev. D **46**, 3720 (1992).
[4] Soudan2 Collaboration, W. W. M. Allison *et al.*, Phys. Lett. B **446**, 1562 (1999).
[5] MACRO Collaboration, M. Ambrosio *et al.*, Phys. Lett. B **434**, 451 (1998).
[6] J. G. Learned, S. Pakvasa, and T. J. Weiler, Phys. Lett. B **207**, 79 (1988).
[7] V. Berger and K. Whisnant, Phys. Lett. B **209**, 365 (1988).
[8] K. Hidaka, M. Honda, and S. Midorikawa, Phys. Rev. Lett. **61**, 1537 (1988).
[9] Kamiokande Collaboration, K. S. Hirata *et al.*, Phys. Lett. B **205**, 416 (1988).
[10] T. K. Gaisser, T. Stanev, S. A. Bludman, and H. Lee, Phys. Rev. Lett. **51**, 223 (1983); G. Barr, T. K. Gaisser, and T. Stanev, Phys. Rev. D **39**, 3532 (1989).
[11] M. Honda, T. Kajita, K. Kasahara, and S. Midorikawa, Phys. Rev. D **52**, 4985 (1995).
[12] V. Agrawal, T. K. Gaisser, P. Lipari, and T. Stanev, Phys. Rev. D **53**, 1314 (1996).
[13] Y. Tserkovnyak *et al.*, hep-ph/9907450.
[14] G. Battistoni *et al.*, Astropart. Phys. **12**, 315 (2000).
[15] P. Lipari, Astropart. Phys. **14**, 171 (2000).
[16] P. Lipari, Astropart. Phys. **14**, 153 (2000).
[17] W. R. Webber *et al.*, in *Proceedings of the 20th ICRC, Moscow*, edited by V. L. Kozyarivsky *et al.* (Nauka, Moscow, 1987), Vol. 1, p. 325.
[18] MASS Collaboration, P. Pappini *et al.*, in *Proceedings of the 23rd ICRC, Calgary*, edited by D. A. Leahy (The University of Calgary, Calgary, 1993), Vol. 1, p. 579.
[19] LEAP Collaboration, W. S. Seo *et al.*, Astrophys. J. **378**, 763 (1987).
[20] IMAX Collaboration, W. Menn *et al.*, Astrophys. J. **533**, 281 (2000).
[21] CAPRICE Collaboration, G. Boezio *et al.*, Astrophys. J. **518**, 457 (1999).
[22] BESS Collaboration, T. Sanuki *et al.*, Astrophys. J. **545**, 1135 (2000).
[23] AMS Collaboration, J. Alcaraz *et al.*, Phys. Lett. B **490**, 27 (2000).
[24] L. H. Smith, Astrophys. J. **180**, 987 (1973).
[25] M. Ryan, J. F. Ormes, and V. K. Balasubrahmanyan, Phys. Rev. Lett. **28**, 985 (1972).
[26] JACEE Collaboration, K. Asakimori *et al.*, Astrophys. J. **502**, 278 (1998).
[27] I. P. Ivanenko *et al.*, in *Proceedings of the 23rd ICRC, Calgary* (Ref. [18], Vol. 2, p. 17).
[28] M. Ichimura *et al.*, Phys. Rev. D **48**, 1949 (1993).
[29] K. Kasahara, in *Proceedings of the 24th ICRC, Rome*, edited by N. Iucci (Istituto Nazionale Fisica Nucleare, Roma, Italy, 1995), Vol. 1, p. 399; see also http://eweb.b6.kanagawa-u.ac.jp/~kasahara/ResearchHome/cosmosHome/
[30] P. Lipari, T. Stanev, and T. K. Gaisser, Phys. Rev. D **58**, 073003 (1998).
[31] Super-Kamiokande Collaboration, T. Futagami *et al.*, Phys. Rev. Lett. **82**, 5194 (1999).
[32] T. K. Gaisser and T. Stanev, Phys. Rev. D **57**, 1977 (1998).